JPET Fast Forward. Published on June 6, 2012 as DOI: 10.1124/jpet.112.194167

TITLE PAGE

An *ex-vivo* perfusion system emulating *in-vivo* conditions in non-cirrhotic and cirrhotic human liver

Thomas Schreiter, Guido Marquitan, Malin Darnell, Jan-Peter Sowa, Martina Bröcker-Preuss, Tommy B. Andersson, Hideo A. Baba, Marcus Furch, Gavin E. Arteel, Zoltan Mathé, Jürgen Treckmann, Guido Gerken, Robert K. Gieseler & Ali Canbay

Clinic for Gastroenterology and Hepatology, Center for Internal Medicine, University Hospital Essen, Essen, Germany (T.S., G.M., J.P.S., G.G., R.K.G., A.C.); Rodos BioTarget GmbH, Medical Park Hannover, Hannover, Germany (M.F., R.K.G.); Dept. of Physiology and Pharmacology, Karolinska Institute, Stockholm, Sweden (M.D., T.B.S.); Dept. of Endocrinology, Dept. of Clinical Chemistry and Laboratory Medicine, University Hospital Essen, Essen, Germany (M.B.P.); Inst. for Pathology and Neuropathology, University Hospital Essen, Germany (H.A.B.); Department of Pharmacology and Toxicology, University of Louisville Health Sciences Center, Louisville, Kentucky, USA (G.E.A.); and Clinic for General, Visceral and Transplantation Surgery, University Hospital Essen, Essen, Germany (Z.M., J.T.)

Primary laboratory of origin:
Clinic for Gastroenterology and Hepatology, Center for Internal Medicine, University Hospital Essen

RUNNING TITLE PAGE

Running title: Perfusion of human liver sections

Corresponding author:

Prof. Ali Canbay, M.D.

Clinic for Gastroenterology and Hepatology

University Hospital Essen

Hufelandstr. 55

45122 Essen, Germany

E-mail: ali.canbay@uni-due.de

Telephone: +49-201-723-84713

Fax: +49-201-723-5719

List of Abbreviations

NC, non-cirrhotic (liver tissue); CL, cirrhotic (liver tissue); AST, aspartate aminotransferase; ALT, alanine aminotransferase; LDH, lactate dehydrogenase; GLDH, glutamate dehydrogenase; γGT, γ-glutamyl transferase; CYP, cytochrome P450; DILI, drug-induced liver injury; HBSS, Hank's balanced salt solution

Counts

Text pages:	20 (Abstract, Introduction, Methods, Results, Discussion)
Tables:	2
Figures:	8
References:	41 (60)
Words in Abstract:	249 (250)
Words in Introduction:	465 (750)
Words in Discussion:	1,475 (1,500)

Recommended section:

Either "Drug Discovery and Translational Medicine" (1st choice) or "Gastrointestinal, Hepatic, Pulmonary, and Renal" (2nd choice)

JPET Fast Forward. Published on June 6, 2012 as DOI: 10.1124/jpet.112.194167
This article has not been copyedited and formatted. The final version may differ from this version.

ABSTRACT

Various models are employed for investigating human liver diseases and for testing new drugs. However, data generated in such models have only limited relevance for the respective *in-vivo* conditions in humans. We here present an *ex-vivo* perfusion system utilizing human liver samples that enables to characterize parameters in a functionally intact tissue context. Resected samples of non-cirrhotic and cirrhotic liver (NC: n=10; CL: n=12) were perfused for 6-h periods. General and liver-specific parameters (glucose, lactate, oxygen, albumin, urea, bile acids); liver enzymes (aspartate aminotransferase, alanine aminotransferase, lactate dehydrogenase, glutamate dehydrogenase, γ-glutamyl transferase); overall (M65) and apoptotic (M30) cell-death markers; as well as indicators of phase-I/phase-II biotransformations were analyzed. The measurement readings closely resembled (patho)physiological characteristics in patients with NC and CL: Mean courses of glucose levels reflected the CL's reduced glycogen storage capability. Furthermore, CL samples exhibited significantly stronger increases in lactate, bile acids, and in the M30/M65 ratio than NC specimens. Likewise, NC samples exhibited more rapid phase-I transformations of phenacetin, midazolam and diclofenac as well as phase I-to-phase II turnover rates of the respective intermediates than CL tissue. Collectively, these findings reveal the better hepatic functionality in NC. Perfusion of human liver tissue with this system emulates *in-vivo* conditions and clearly discriminates between non-cirrhotic and cirrhotic tissue. Employing this highly reliable device for basic hepatologic research and for testing the safety/ toxicity, the pharmacokinetics/ pharmacodynamics and the efficacies of novel therapeutic modalities thus promises to generate superior data compared to those obtained *via* existing economic perfusion systems.

JPET Fast Forward. Published on June 6, 2012 as DOI: 10.1124/jpet.112.194167
This article has not been copyedited and formatted. The final version may differ from this version.

INTRODUCTION

Unpredicted drug-induced liver injury (DILI) accounts for termination of ~22% of drugs in clinical trials and for ~32% withdrawals of approved drugs (Watkins, 2011). Although animal models have long been used for mimicking physiological and pathophysiological conditions in human liver, data gathered from such models not always match humans. Ethical considerations of course limit the use of human test subjects for such studies (Cheng et al., 2011). There is therefore a key need for models that better predict DILI in humans. Furthermore, models that also more reliably predict drug metabolization, pharmacodynamics, pharmacokinetics and pharmacogenomics are a cornerstone of pharmaceutical development (Watkins, 2011; Liew et al., 2011).

Several established *in-vitro* models employ primary human hepatocytes as well as isolated hepatic tissue to evaluate physiological, pathophysiological and pharmacological characteristics (Gebhardt et al., 2003; Hewitt et al., 2007; Gómez-Lechón et al., 2008). Primary hepatocytes grown in suspension or in 2-dimensional culture conditions rapidly lose important phenotypes found *in vivo* (e.g., phase I and II metabolism). Although some culture systems provide 3D scaffolds that maintain hepatocyte function and metabolism for longer periods of time (Gerlach, 2006; Zeilinger et al., 2011; Balmert et al., 2011; Funatsu et al., 2001), the complexity of the intact organ with multiple cell types is not recapitulated. Cultured hepatic tissue (e.g., liver slices) addresses some of the concerns of cell culture, but also has limitations. Specifically, the oxygen/nutrient gradient normally found in the liver lobule as an effect of blood flow is not present in cultured slices.

An *ex-vivo* model that bypasses some of the limitations raised above is machine-perfused organs. In such a system, the hepatic architecture is maintained, as well as

the lobular flow of oxygen and nutrients. Isolated perfused livers from research animals (e.g., pig, sheep or rat) are often used for for studying hepatotoxicity and metabolism (Grosse-Siestrup et al., 2002; Thewes et al., 2007; Ali et al., 2000; Bessems et al., 2006). Machine perfusion of human tissue is generally performed to maintain an organ's quality until transplantation and to minimize reperfusion damage (Dutkowski et al., 2008; Vogel et al., 2010; Monbaliu and Brassil, 2010), with few if any studies employing such a system to characterize hepatic responses.

The first goal of this work was to therefore develop an *ex-vivo* perfusion system of human liver tissue. We present an economic closed-circuit perfusion system that maintains a piece of human liver up to a weight of 55 g viable for >6 hrs. We compared the responses in normal and cirrhotic liver tissue in order to develop a paradigm in which the characteristics of healthy and diseased livers can be compared. The functional parameters obtained throughout the perfusion period indicate that this setup will enable (patho)physiological, pharmacodynamic, pharmacokinetic, pharmacogenomic and toxicological analyses in an environment mimicking the hepatic *in-vivo* situation as closely as possible.

MATERIAL AND METHODS

Patients and liver samples. All patients provided written informed consent according to the Helsinki declaration of 1995, and the study protocol conformed to the guidelines of the ethics committee of the University Hospital Essen (File number: 09-4252). Non-cirrhotic liver tissue (NC, n=10) was mostly obtained from liver portions that had been partially resected due to different entities of liver-metastasized neoplasms (Tab. 1), with an ample circumference of surrounding healthy tissue. While the diseased tissue was forwarded to the pathologist, adjacent unaffected tissue was transferred to the laboratory, stripped of any remnants of macroscopically visible pathologic areas, and then connected to the perfusion system (see below). During this procedure tissue pieces were collected for paraffin embedding (Roti®-Histofix 4%, Carl Roth GmbH & Co.KG, Karlsruhe, Germany) and cryopreservation for subsequent histological analysis. A second sampling was performed at the end of the perfusion period. Cirrhotic liver tissue (CL, n=12) was mainly derived from the left lobe of whole liver explants in the course of complete orthotopic liver transplantation in patients with hepatitis C, primary biliary cirrhosis or ethanol toxicity (Tab. 1).

Liver perfusion system. The perfusion system was designed as a closed circuit providing a constant flow rate, being supplied with nutrients and oxygen, to liver samples of 20–55 g (for a schematic drawing, see Figure 1; for a photograph of the actual setup cf. Supplementary Figure 1). A pump drive with two peristaltic heads (Masterflex *via* Novodirect, Kehl, Germany) was used for the bidirectional transport of the perfusion medium. Medium was oxygenated by a commercially available aquarium pump (Hagen, Holm, Germany) and routed through a custom-built glass heating coil flowed with water kept at 40°C *via* an external heating outlet (Julabo,

Seelbach, Germany). The fluid's pressure was measured manometrically (VBM Medizintechnik, Sulz, Germany) and values ranged from 40 to 100 mm Hg. Before entering the liver sample, the perfusion fluid was degassed by means of a bubble trap (Stem Cell Systems, Berlin, Germany). A three-way valve was installed thereafter for collecting perfusion medium before passing the liver sample. The specimen was connected *via* four branches of the circuit tubing, ending in venous catheters, and the perfusate efflux was collected in a bowl and re-conveyed to the medium reservoir. This connection was furnished with another three-way valve for sampling after liver passage, and for applying any agents. Liver specimens were maintained at 37°C in a water bath.

Experimental perfusion. Onset of the perfusion procedure ranged from 1 h to 19 h (5.6 ± 1.5) after tissue retrieval. First, the liver piece was connected to the perfusion circuit *via* 2-4 cannulas – dependent on available vessels – adhered into portal or central veins (macroscopically indiscernible) by the tissue adhesive, Histoacryl (Braun, Melsungen, Germany). Second, the surgical cutting area was sealed with tissue adhesive. The liver piece was then rinsed with approx. 500 ml of Hank's balanced salt solution (HBSS; PAA, Cölbe, Germany) supplemented with 20 mM 4-(2-hydroxyethyl)-1-piperazine-ethanesulfonic acid (HEPES; PAA) and 2 U/ml heparin (Ratiopharm, Ulm, Germany) for removing residual blood, whereupon exchanging the perfusion medium to 250 ml Williams' medium E (Biochrom, Berlin, Germany) containing 20 mM HEPES. The first 50 ml volume of the perfusate was discarded for removing as much residual blood as possible and to establish a standardized zero point with fresh perfusion medium. The circuit was closed by placing the effluent tubing into the medium reservoir (Figure 1). After the initial sampling the time

JPET Fast Forward. Published on June 6, 2012 as DOI: 10.1124/jpet.112.194167
This article has not been copyedited and formatted. The final version may differ from this version.

measurement was started and flow rates were adjusted to obtain an appropriate pressure of about 50 mmHg (i.e., 40 or 50 ml/min). The perfusion was run for 6 h, and perfusate samples were collected hourly. For determination of CYP activity, additional samples were taken at 0.25 and 0.5 h. Glucose and lactate concentrations as well as pH and pO_2 (general metabolism) were measured instantly on the blood gas analyzer ABL715 (Radiometer, Willich, Germany), and the pH was adjusted to 7.3-7.4 by adding 1-2 mL of 8.4% sodium bicarbonate solution (Braun) to the perfusate as needed. When small (< 20 g) pieces of liver were employed, the initial pH turned alkaline; in these cases 2–3 mM of sodium dihydrogen phosphate (Sigma-Aldrich, Munich, Germany) were added. In case the glucose concentration decreased below 40 mg/dL, the perfusate was supplemented with 0.75–1.0 ml of a 40% glucose solution (Braun) corresponding to 150–200 mg/dL glucose. At termination of the experiment, 2 mL of trypan blue (Sigma-Aldrich) were added and perfused for 10 min to allow for evaluation of perfusion efficiency and identification of the perfused tissue areas. Liver specimens were finally cut into 1-cm slices, and areas of interest were either stored in 4% paraformaldehyde for paraffin embedding with subsequent histochemical staining, or in liquid nitrogen prior to cryosectioning.

Biochemical parameters and cell death markers. For determining biochemical parameters, perfusate samples were stored at 4°C overnight and then transferred to the Dept. of Clinical Chemistry and Laboratory Medicine (University Hospital Essen). Activities of ALT, AST, γGT, GLDH, and LDH were determined on the ADVIA 1800 Chemistry System (Siemens Healthcare Diagnostics, Eschborn, Germany) using the respective assay cassettes. Human albumin was quantified with the AssayPro Human Albumin ELISA kit (St. Charles, MO, USA).

JPET Fast Forward. Published on June 6, 2012 as DOI: 10.1124/jpet.112.194167
This article has not been copyedited and formatted. The final version may differ from this version.

For comparability, measurements were normalized to the per-gram weight of the different liver specimens. Glucose turnover was calculated by subtracting the initial glucose contents of the culture medium from the perfusates' concentrations at times of sampling. Positive values were defined as production or release of a compound while negative values were assumed to reflect consumption – except for oxygen, whose consumption was calculated by determining the partial pressure deviation in the perfusate before entering, and after exiting, the liver specimen (in mm Hg), multiplied by the flow rate (in dL/min) and the Henry constant (0.3 mL x dL^{-1} x mm Hg^{-1}).

Overall cell death and apoptosis rates were determined with the M65 and M30 ELISA kits (Peviva, Bromma, Sweden) according to the manufacturer's instruction.

Acitivity of cytochrome P450 (CYP). The CYP activity was assessed by adding a CYP substrate cocktail consisting of phenacetin (CYP1A1), midazolam (CYP3A4) and diclofenac (CYP2C9) to the medium reservoir directly before starting the time measurement of each experiment. Phenacetin and diclofenac (both from Sigma-Aldrich) were prepared as stock solutions of 80 and 40 mmol/L, respectively, in dimethyl sulfoxide (DMSO), and were diluted in culture medium to final concentrations of 26 µM or 9 µM, respectively, in the perfusion circuit. Midazolam was provided as an aqueous solution (Dormicum®, Roche Pharma, Grenzach-Wyhlen, Germany) at 13.8 mM (= 5 mg/ml) and diluted to a perfusion concentration of 3 µM. Samples of 200 µl were taken from below the bubble trap at the indicated time points in the experimental procedure and stored at -20°C until further processing.

JPET Fast Forward. Published on June 6, 2012 as DOI: 10.1124/jpet.112.194167
This article has not been copyedited and formatted. The final version may differ from this version.

The metabolites N-(4-hydroxyphenyl)acetamide (acetaminophen, paracetamol), 1'-hydroxymidazolam and 4'-hydroxydiclofenac were analyzed by liquid chromatography/mass spectrometry. Before analysis, 50 µl of the sample and standard were precipitated in 150 µl ice-cold acetonitrile. The samples were placed in the freezer (-20 ºC) for 20 min and then centrifuged for 20 min at 4000 g and 4 ºC. 40 µl supernatant was mixed with 60 µl internal standard or diluted 10 times before addition of the internal standard. The internal standard consisted of 200 nM 1'-hydroxymidazolam-^{13}C3 (Toronto Research Chemicals, Toronto, Canada), paracetamol-d4 and 4'-hydroxydiclofenac-^{13}C6 (Gentest, Woburn, USA). The liquid chromatography system consisted of a HTS PAL injector (CTC Analytics, Zwingen, Switzerland) combined with an HP 1100 LC binary pump and column oven (Agilent Technologies, Waldbronn, Germany). The separation was performed on a reversed 20 phase HyPurity C18 analytical column (50×2.1 mm, 5 µm; Thermo Scientific, Runcorn, UK) at 40°C and with a flow rate of 750 µL/min. The mobile phases consisted of 0.1% (v/v) formic acid in 5% acetonitrile (A) and 0.1% (v/v) formic acid in 95% acetonitrile (B). Detection was performed with a triple Quadrupole Mass Spectrometer (API4000), equipped with an electrospray interface (Applied Biosystems/MDS Sciex, Concorde, Canada). Instrument control, data acquisition and data evaluation were performed using Applied Biosystems/MDS Sciex Analyst 1.4 software.

Immunohistochemical staining of cytochrome P450 (CYP) isoenzymes. Sections of embedded liver tissue were subjected to deparaffinization and antigen retrieval using citric buffer with heating in a microwave oven for 20 min. Antibodies raised in rabbit against CYP1A1, CYP3A4 and CYP2C9 (Abcam, Cambridge, UK) were diluted in phosphate buffered saline (PAA; 1:10, 1:1000 and 1:100, respectively) and

sections were incubated for 1 h. Immunohistochemistry was performed with the HISTAR detection kit (AbD Serotec, Düsseldorf, Germany) which includes 3,3'-diaminobenzidine as chromogenic dye. Cell nuclei were counterstained with hematoxylin (Sigma-Aldrich, Munich, Germany) and digital images were captured on the Axioplan microscope with camera Axiocam HRc (Zeiss, Jena, Germany).

Statistical analysis. Parameters, areas under-the-curve (AUCs), Pearson correlations and two-way ANOVA statistical analyses were calculated and graphically displayed by GraphPad Prism 5 (GraphPad Software, La Jolla, CA, USA). Fold changes during perfusion were calculated by setting the 1-h parameter values to one. Maximal changes were determined between the lowest and highest value during perfusion, regardless of the time point. All data are given as means ± SEM. Statistical significance was assumed at $p \leq 0.05$. Grubbs test was performed in Excel 2007 (Microsoft Corp., USA).

JPET Fast Forward. Published on June 6, 2012 as DOI: 10.1124/jpet.112.194167
This article has not been copyedited and formatted. The final version may differ from this version.

RESULTS

General patients' characteristics in NC and CL

NC liver specimens were obtained from resections on 50 % female and 50 % male patients (mean age: 57.2 ± 3.5 y). Liver explants of CL were derived from 75% male and 25% female patients (mean age: 53.3 ± 2.7 y [n.s.]). The underlying diseases varied strongly between the groups (Tab. 1).

Histochemical tissue characterization before and after perfusion

Figure 2 shows representative photomicrographs (hematoxylin and eosin; H&E) of livers from NC (Panels A-C) and CL (Panels D-F) at explant (Panels A and D) and after 6 h of perfusion (Panels B and E). There was no detectable *ex-vivo* cell death in the samples immediately after explant in either group (Panels A and D). Sections of NC liver tissue (Panel B) and CL liver tissue (Panels E) showed no major cell damage in the areas that were perfused for 6 h, but showed large areas of necrosis in the regions that were not machine perfused (Panels C and F).

General metabolic characteristics in NC and CL specimens

Time courses of glucose metabolism (production *vs*. consumption), lactate production and oxygen consumption were recorded (Figure 3). NC tissues provided a rather stable amount of glucose throughout the perfusion process with a maximum of 1.48 ± 0.48 mg x dL^{-1} x g^{-1} at 2 h (Figure 3A). In contrast, CL tissues tended to switch to glucose consumption 1–4 h after the initiation of perfusion; the minimum value in this group was at the end of the perfusion time -1.83 ± 1.87 mg x dL^{-1} x g^{-1} (Figure 3A). Thus, glucose production was about 4.5 times higher in NC as derived from the

JPET Fast Forward. Published on June 6, 2012 as DOI: 10.1124/jpet.112.194167
This article has not been copyedited and formatted. The final version may differ from this version.

AUCs (Tab. 2A). Although lactate production increased linearly in both groups (Figure 3B), the slope in CL was steeper when compared to NC and differed significantly ($p<0.001$; Table 2B), indicating a higher production rate in CL tissue. Lactate values increased by 3.4 ± 0.2 fold for NC and by 4.6 ± 0.2 fold for CL during the course from 1 h to 6 h. Oxygen consumption did not differ between the groups and remained largely constant throughout the observation period, with a maximum of 1.6 ± 0.3 µL x min^{-1} x g^{-1} at 4 h for NC tissue (Figure 3C).

Urea, albumin and bile acids in NC and CL specimens

The rate of urea production increased in both NC and CL tissues over the course of the perfusion (Figure 4A) with a fold change of 3.2 ± 0.3 and 2.6 ± 0.3 between 1 h and 6 h for NC and CL, respectively. The mean concentrations rose by 0.134 ± 0.028 mg x dL^{-1} x g^{-1} for NC and 0.092 ± 0.012 mg x dL^{-1} x g^{-1} for CL tissue within 6 h corresponding to comparable slope values (Tab. 2B). The pattern of albumin production was also similar for NC and CL tissue (Figure 4B) presenting fold changes of 2.0 ± 0.1 and 1.5 ± 0.1, respectively. The maximal gains in albumin concentrations were 2.35 ± 0.5 µg x mL^{-1} x g^{-1} for NC and 0.932 ± 0.279 µg x mL^{-1} x g^{-1} for CL within 6 h. The secretion of bile acids increased during the perfusion time with nearly matching rates (Tab. 2B), although the initial concentration of bile acids was higher in the CL group and remained significantly elevated at all times ($p=0.0119$) (Figure 4C). Bile acids increased by 5.9 ± 1.8 fold for NC and by 1.9 ± 0.2 for CL between 1 h and 6 h. As one non-cirrhotic sample presented more than four times higher values than the means of all others, we removed the bile acid data of this sample from the analysis (the graph and the *p*-value representing the complete data set, including this patient, are given in Supplementary Figure 2).

JPET Fast Forward. Published on June 6, 2012 as DOI: 10.1124/jpet.112.194167
This article has not been copyedited and formatted. The final version may differ from this version.

Liver enzymes are elevated in NC *vs*. CL

In order to assess the maintenance of liver cell integrity during perfusion, established markers of liver damage were determined in the perfusate (Figure 5). In CL tissues, slight and consistent increases in the activities of all liver enzymes tested for were observed over the perfusion time. The elevations of values in CL were 3.8 ± 0.4 fold for AST, 2.6 ± 0.4 fold for ALT, 3.4 ± 0.3 fold for LDH, 10.6 ± 2.6 fold for GLDH and 1.9 ± 0.4 fold for γGT from 1 h to 6 h. In contrast, beginning at 2–3 h after the onset of perfusion, NC livers exhibited a stronger increase in these parameters, leading to significant differences for ALT, GLDH and γGT between the groups. Between 1 h and 6 h of perfusion, the values in NC rose by 12.4 ± 4.6 fold for AST, 18.8 ± 8.9 fold for ALT, 10.6 ± 3.5 fold for LDH and 17.8 ± 4.4 fold for GLDH. In NC specimens, the release of γGT plateaued ~4–5 h after the initiation of perfusion and slightly dropped during the last hour. Thus, the maximal elevation of 3.4 ± 0.7 fold for γGT was found after 5-h perfusion.

Ratio of apoptosis to necrosis is more pronounced in CL

As a consequence of hepatocellular cell death, intracellular proteins like cytokeratin 18 are released into the extracellular matrix. Only during apoptosis a neoepitope of CK18 – M30 – is generated by caspase cleavage. In the perfusate, the M65 ELISA detects the total amount of cell death while the M30 ELISA specifically accounts for apoptosis (Figure 6). M65 mean values ranged from 786 ± 229 U x L^{-1} x g^{-1} in NC liver tissue after 1 h to 1611 ± 489 U x L^{-1} x g^{-1} after 6 h of perfusion resulting in a fold change of 2.8 ± 0.9 (Figure 6A). Mean values for CL tissue started with 1351 ± 633 U

JPET Fast Forward. Published on June 6, 2012 as DOI: 10.1124/jpet.112.194167
This article has not been copyedited and formatted. The final version may differ from this version.

x L^{-1} x g^{-1} after 1 h and plateaued after 4 h with a maximum of 2706 ± 1487 U x L^{-1} x g^{-1} at 6 h of perfusion which is equivalent to a 1.7 ± 0.2 fold change. The courses of M30 indicated a stronger slope for CL with fold changes of 2.9 ± 0.8 for NC and of 3.0 ± 0.5 for CL tissue (Figure 6B). While the courses of M65 or M30 did not differ significantly, the M30/M65 ratio was significantly higher in the CL specimens (p=0.0066, Figure 6C). This ratio remained fairly stable at 2% for NC throughout perfusion, it increased for CL from 3.2% (1 h) to 5.4% (6 h).

Metabolic activity of cytochrome P450 enzymes differ between NC and CL

As a more detailed measure of hepatic function, we investigated phase-I conversions of three model cytochrome P450 substrates. In the initial 30-min interval, OH-midazolam and OH-diclofenac were formed quite rapidly, but dropped continuously thereafter (CYP3A4, Figure 7, B/E; CYP2C9, Figure 7, C/F) due to formation of the phase-II products. The glucuronides of OH-midazolam and OH-diclofenac were identified by qualitative Q-TOF analysis (data not shown). The formation rates of OH-midazolam, as calculated from the linear sections at the beginning of the curves, were 15.9 ± 5.2 and 6.1 ± 3.7 nM x g^{-1} x h^{-1} for NC or CL tissue, respectively; the accordant formation rates of OH-diclofenac resulted in 0.127 ± 0.044 or 0.062 ± 0.019 µM x g^{-1} x h^{-1}, respectively. The phase-I metabolite of phenacetin was built within the first 2 h and then plateaued (CYP1A1/1A2, Figure 7, A/D). The formation rates of paracetamol were 0.306 ± 0.09 *vs*. 0.064 ± 0.033 µM x g^{-1} x h^{-1} for NC or CL tissue, respectively. Furthermore, the slopes of CYP1A1/1A2 and CYP3A4 within the linear range were not significant different from zero for CL tissue. As a result of overlapping phase-I and phase-II reactions, the courses of NC and CL tissue intersected for CYP3A4 and CYP2C9 activity once the phase-I reactions were

completed in NC. To quantify the extent of both reactions for NC and CL, the areas under the curves (AUCs) were calculated before and after this intersection (Figure 7, G-J). For CYP1A1/1A2 activity a corresponding AUC was defined when the curve reached the plateau in NC. In CL tissue, phase-I products of all three CYP substrates were generated much slower than in NC tissue, thus leading to deviations in the AUCs from -69.3 to -24.2 % (Figure 7, G-J). Additionally, the protracted presence of phase-I products for CL tissue – with higher AUCs up to 53.8 % – also suggests a much slower formation of phase-II products in CL. None of the observed differences for CYP activities in NC and CL tissue reached statistical significance.

Immunohistochemical stains of the three CYP isoenzymes (Figure 8) revealed stronger enzyme presence in NC compared to CL tissue before the experiment and slightly reduced amounts after 6 h of perfusion in both types of tissue. While the intensity within positive hepatocytes was roughly the same for NC and CL, the positive tissue area was clearly smaller in CL. Thus, low CYP activity in the CL patients can likely be attributed to diminished intact parenchymal cell mass in cirrhotic liver tissue.

JPET Fast Forward. Published on June 6, 2012 as DOI: 10.1124/jpet.112.194167
This article has not been copyedited and formatted. The final version may differ from this version.

DISCUSSION

Model systems for evaluating drugs generally employ single-type cell cultures or animal models (Groneberg et al., 2002; Gómez-Lechón et al., 2003; Elaut et al., 2006). Although valuable, both of which have their limitations. Specifically, cell lines sometimes critically differ from their healthy counterparts and – on the opposite side of the spectrum – even humanized (chimeric) animal models do not entirely reflect the actual situation in patients: They may differ in their (patho)physiologies, modes of infection, pharmacological metabolization and toxicity characteristics – and are, moreover, especially fragile (Tateno et al., 2004; Dandri et al., 2005; Vanwolleghem et al., 2010; Lütgehetmann et al., 2012). Such limitations may be remedied with a suitable human-based perfusion system, even more so if such a system can maintain certain pathological conditions. This demand can be met with the presented perfusion system.

Comparison with other ex-vivo systems

Our system for *ex-vivo* human liver perfusion offers a host of research applications combined with a strong economic advantage compared to perfusion machines that are usually employed for preserving organ transplants (Taylor and Baicu, 2010). Generally, such systems cool down the tissue to avoid degeneration and cell death, employ expensive protective solutions to limit cold ischemia/reperfusion injury, and require a sterile transportation device. In contrast, our system avoids expensive factors and components that are required for prolonged graft storage but are not mandatory for short-term tissue survival.

In order to compare the tissue's synthesis performance with other hepatocyte culture systems, reported 1-day production rates were converted into hourly values.

JPET Fast Forward. Published on June 6, 2012 as DOI: 10.1124/jpet.112.194167
This article has not been copyedited and formatted. The final version may differ from this version.

Corresponding parameters obtained in NC liver tissue were calculated by using the slopes of the curves (urea, albumin and lactate) or the AUC (glucose). Our values were normalized per gram of tissue, so that our calculations are based on 5 x 10^7 cells/cm^3 of liver (as determined in a biopsy punch; not shown). *In-vivo* hepatic production rates of urea (65 µg/h per 10^7 cells) and albumin (20-30 µg/h per 10^7 cells) were reported previously (Bhatia et al., 1999). Another important factor is that hepatocytes account for ~80% of the cellular volume and for ~60% of the hepatic cell number (Kmieć, 2001), while liver cells cultured in 2D or 3D environments mainly consist of hepatocytes. Our perfusion system revealed a mean urea production of 7.1 µg/h per 10^7 cells and a mean albumin production of 11.7 µg/h per 10^7 cells. When considering the perfused areas, these albumin values match with *in-vivo* data, while the low urea production likely reflects reduced protein degradation. Bioreactor cultures produced 44.8 µg/h per 10^7 cells of urea and 2 µg/h per 10^7 cells of albumin on day 1 (Zeilinger et al., 2011) or, under serum-free conditions, 41.8 µg/h per 10^7 cells of urea and 0.3 µg/h per 10^7 cells of albumin (Mueller et al., 2011). The discrepancy in albumin production may be explained by the fact that the detectable amount of albumin (and other proteins) under serum-free conditions is reduced by coating of the capillaries. On day 1, comparable values of urea (7.5 µg/h per 10^7 cells) and albumin (3.8 µg/h per 10^7 cells) were actually reported in 2-D cultures (Bhogal et al., 2011). Glucose release was calculated as 92 µg/h per 10^7 cells in the bioreactors (with high inter-sample variances), as opposed to 428 µg/h per 10^7 cells in perfused liver specimens. Lactate production in bioreactors was 60.2 µg/h per 10^7 cells, in contrast to 160 µg/h per 10^7 in our system. Whether this discrepancy indicates elevated hepatocyte activity or insufficient oxygen supply will be subject to future investigation.

Comparison with the in-vivo situation

Using the system described herein, the parameters measured in non-cirrhotic and cirrhotic tissue closely resembled the (patho)physiological characteristics *in vivo*.

Increased lactate and bile acid production rates paralleled the situation in patients with CL (Almenoff et al., 1989; Bernal et al., 2002; Pennington et al., 1977; Akashi et al., 1987). The fact that cirrhotic samples initially showed increased glucose production, which later switched to consumption (as opposed to NC samples with a constant production rate) reflects the reduced glycogen storage capacity of cirrhotic livers (Krähenbühl et al., 2003).

In NC, parameters of liver damage (AST, ALT, LDH, GLDH, γGT) rose much more clearly than in CL. Likewise, chronic liver damage clinically leads to a continuous decline in cell numbers. This is paralleled by a decreasing release of liver enzymes (Canbay et al., 2009), which is sharply contrasted by the sudden and extensive organ damage in acute liver failure (Bechmann et al., 2010). Consequently, high ALT and AST values are associated with better outcome upon acute liver failure (Canbay et al., 2009).

Limitations

Applications of the novel system may be limited by the availability of appropriate tissue samples. Our perfusion studies were performed at a major hepatological center with a highly experienced liver transplantation department and well-attuned personnel. In contrast, smaller sites may not have access to sufficiently large specimens of patients' livers and the desirable infrastructural preconditions, which is a bottleneck situation that also applies to the provision of human samples for

isolating primary liver cells. Importantly however, this limitation does not argue against employing the novel system to improve the conditions for basic and applied hepatologic research in suitable clinical settings.

Absence of other organs or organ systems as for example the immune system, confine the available information to liver related processes. Though, this limitation is also present in all other *in-vivo* models.

Another current limitation arises from incomplete tissue perfusion under the conditions employed; according to trypan-blue staining, 50-80% of the tissue was adequately perfused. Nevertheless, data normalized to the liver samples' weights were consistent within the NC and CL groups with only small standard deviations, so that comparable tissue fractions were perfused in each sample. During the perfusion period, liver samples showed a trend towards cell damage at the later points in time. Both this drawback as well as the overall *ex-vivo* perfusion time shall be further improved by enhancing oxygen transport and/or delivery as well as by continuously providing glucose and additional nutrients.

Benefits

The novel perfusion system offers some decisive benefits – e.g., for preclinical drug testing in an original, patient-derived setting. It will thus be especially valuable for investigations requiring intact hepatocyte polarity and/or the hepatocytes' interplay with nonparenchymal cell species. Rapid phase-I conversions of three human-relevant CYP substrates clearly proved that the hepatocytes were functionally active and performed detoxification reactions. Moreover, rapid consumption of the midazolam and diclofenac phase-I metabolites confirmed the hepatocytes' intact phase-II metabolism. Both types of reactions were more pronounced in NC than in

CL specimens. These results are in line with the *in-vivo* situation in such patients and are a considerable improvement over most culture systems. For example, a similar CYP testing setup with bioreactor-cultured primary human hepatocytes exhibited more than two-fold slower phase-I formation clearances and significantly lower phase-II reactions (Zeilinger et al., 2011; Mueller et al., 2011).

A comparable perfusion system published previously (Melgert et al., 2001) varied in some aspects: First, their system differed in oxygenation and usage of perfusion solution (Krebs-Henseleit buffer), and tissue pieces were stored in cold UW solution for 6-39 h prior to perfusion. In contrast, our procedure employed a cold-storage period between tissue retrieval and onset of perfusion of 1-19 h (5.6 ± 1.5). Second, their functional assessment of liver tissue was performed with fewer samples (7 NC; 4 CL) for 1 h as opposed to our perfusion of 10 or 12 specimens, respectively, for 6-h periods thus allowing for measurements or treatments that require prolonged incubation or reaction times.

The system introduced herein thus offers substantial advantages for the basic characterization of liver function. It opens up options for the *ex-vivo* evaluation of metabolic conditioning as well as for investigating innovative treatments for non-alcoholic steatohepatitis, the viral hepatitides and hepatocellular carcinoma as increasingly relevant disease entities in countries with Western(ized) lifestyle habits as well as, partly, in Middle-Eastern and North-African countries (Angulo, 2007; Nelson et al., 2011; Rahbari et al., 2011; Ertle et al., 2011). Moreover, the system can also be utilized for evaluating investigational new drugs at close-to-human conditions with higher reliability.

JPET Fast Forward. Published on June 6, 2012 as DOI: 10.1124/jpet.112.194167
This article has not been copyedited and formatted. The final version may differ from this version.

Conclusions

By introducing this perfusion system and the baseline characterization of liver specimens derived from different disease entities, we hope to open up new possibilities not only for hepatologic investigations. Continued improvement as to ease of handling, oxygen/nutrient supply as well as complementary data on liver tissue parameters may enable a wider range of applications. The informative power of this *ex-vivo* perfusion system may also be enhanced by integrating an existing cutting-edge multi-gene expression signature that excellently predicts hepatotoxicity (Cheng et al., 2011). Such a follow-up system may pinpoint undesired or dangerous phase-I and/or phase-II metabolites of investigational new drugs with high reliability. Both the present-stage system as well as its successors are anticipated to provide excellent models for investigating the overall performances and adverse effects of promising new drug candidates in the context of liver disease.

ACKNOWLEDGEMENTS

All authors are most grateful to the cooperative surgical teams, as well as to Svenja Sydor, Anja Beilfuss, Dr. Ruth Bröring, Melanie Lutterbeck, Ivonne Nel, Achim Konietzko and Paul Manka who extensively participated in retrieving the liver specimens including many night shifts. They are the backbone of the work presented herein. We greatly appreciate the expert technical assistance by Lena Wingerter, Dorothe Möllmann, and Martin Schlattjan and we are also indebted to Dr. Frank Petrat for enabling blood gas analysis.

AUTHORSHIP CONTRIBUTIONS

Participated in research design: Schreiter, Marquitan, Sowa, Gieseler.

Conducted experiments: Schreiter, Marquitan.

Contributed new reagents or analytic tools: Darnell, Andersson, Bröcker-Preuss, Baba, Mathe, Treckmann.

Performed data analysis: Schreiter, Marquitan, Darnell, Sowa.

Wrote or contributed to the writing of the manuscript: Schreiter, Darnell, Sowa, Andersson, Furch, Arteel, Gerken, Gieseler, Canbay.

REFERENCES

Akashi Y, Miyazaki H, Yanagisawa J, and Nakayama F (1987) Bile acid metabolism in cirrhotic liver tissue--altered synthesis and impaired hepatic secretion. *Clin Chim Acta* 168:199–206.

Ali AM, Rossouw HC, Silove M, and Walt JG (2000) Development of an improved technique for the perfusion of the isolated caudal lobe of sheep liver. *Exp Physiol* 85:469–478.

Almenoff PL, Leavy J, Weil MH, Goldberg NB, Vega D, and Rackow EC (1989) Prolongation of the half-life of lactate after maximal exercise in patients with hepatic dysfunction. *Crit Care Med* 17:870–873.

Angulo P (2007) Obesity and nonalcoholic fatty liver disease. *Nutr Rev* 65:S57–63.

Balmert SC, McKeel D, Triolo F, Gridelli B, Zeilinger K, Bornemann R, and Gerlach JC (2011) Perfusion circuit concepts for hollow-fiber bioreactors used as in vitro cell production systems or ex vivo bioartificial organs. *Int J Artif Organs* 34:410–421.

Bechmann LP, Jochum C, Kocabayoglu P, Sowa J-P, Kassalik M, Gieseler RK, Saner F, Paul A, Trautwein C, Gerken G, and Canbay A (2010) Cytokeratin 18-based modification of the MELD score improves prediction of spontaneous survival after acute liver injury. *J Hepatol* 53:639–647.

Bernal W, Donaldson N, Wyncoll D, and Wendon J (2002) Blood lactate as an early predictor of outcome in paracetamol-induced acute liver failure: a cohort study. *Lancet* 359:558–563.

Bessems M, 't Hart NA, Tolba R, Doorschodt BM, Leuvenink HGD, Ploeg RJ, Minor T, and van Gulik TM (2006) The isolated perfused rat liver: standardization of a time-honoured model. *Lab Anim* 40:236–246.

Bhatia SN, Balis UJ, Yarmush ML, and Toner M (1999) Effect of cell-cell interactions in preservation of cellular phenotype: cocultivation of hepatocytes and nonparenchymal cells. *FASEB J* 13:1883–1900.

Bhogal RH, Hodson J, Bartlett DC, Weston CJ, Curbishley SM, Haughton E, Williams KT, Reynolds GM, Newsome PN, Adams DH, and Afford SC (2011) Isolation of primary human hepatocytes from normal and diseased liver tissue: a one hundred liver experience. *PLoS ONE* 6:e18222.

Canbay A, Jochum C, Bechmann LP, Festag S, Gieseler RK, Yüksel Z, Lütkes P, Saner FH, Paul A, and Gerken G (2009) Acute liver failure in a metropolitan area in Germany: a retrospective study (2002 - 2008). *Z Gastroenterol* 47:807–813.

Cheng F, Theodorescu D, Schulman IG, and Lee JK (2011) In vitro transcriptomic prediction of hepatotoxicity for early drug discovery. *J Theor Biol* 290:27–36.

Dandri M, Volz TK, Lütgehetmann M, and Petersen J (2005) Animal models for the study of HBV replication and its variants. *J Clin Virol* 34 Suppl 1:S54–62.

Dutkowski P, de Rougemont O, and Clavien P-A (2008) Machine perfusion for "marginal" liver grafts. *Am J Transplant* 8:917–924.

Elaut G, Papeleu P, Vinken M, Henkens T, Snykers S, Vanhaecke T, and Rogiers V (2006) Hepatocytes in suspension. *Methods Mol Biol* 320:255–263.

Ertle J, Dechêne A, Sowa J-P, Penndorf V, Herzer K, Kaiser G, Schlaak JF, Gerken G, Syn W-K, and Canbay A (2011) Non-alcoholic fatty liver disease progresses to hepatocellular carcinoma in the absence of apparent cirrhosis. *Int J Cancer* 128:2436–2443.

Funatsu K, Ijima H, Nakazawa K, Yamashita Y, Shimada M, and Sugimachi K (2001) Hybrid artificial liver using hepatocyte organoid culture. *Artif Organs* 25:194–200.

Gebhardt R, Hengstler JG, Müller D, Glöckner R, Buenning P, Laube B, Schmelzer E, Ullrich M, Utesch D, Hewitt N, Ringel M, Hilz BR, Bader A, Langsch A, Koose T, Burger H-J, Maas J, and Oesch F (2003) New hepatocyte in vitro systems for drug metabolism: metabolic capacity and recommendations for application in basic research and drug development, standard operation procedures. *Drug Metab Rev* 35:145–213.

Gerlach JC (2006) Bioreactors for extracorporeal liver support. *Cell Transplant* 15 Suppl 1:S91–103.

Gómez-Lechón MJ, Castell JV, and Donato MT (2008) An update on metabolism studies using human hepatocytes in primary culture. *Expert Opin Drug Metab Toxicol* 4:837–854.

Gómez-Lechón MJ, Donato T, Ponsoda X, and Castell JV (2003) Human hepatic cell cultures: in vitro and in vivo drug metabolism. *Altern Lab Anim* 31:257–265.

Groneberg DA, Grosse-Siestrup C, and Fischer A (2002) In vitro models to study hepatotoxicity. *Toxicol Pathol* 30:394–399.

Grosse-Siestrup C, Pfeffer J, Unger V, Nagel S, Witt C, Fischer A, and Groneberg DA (2002) Isolated hemoperfused slaughterhouse livers as a valid model to study hepatotoxicity. *Toxicol Pathol* 30:749–754.

Hewitt NJ, Lechón MJG, Houston JB, Hallifax D, Brown HS, Maurel P, Kenna JG, Gustavsson L, Lohmann C, Skonberg C, Guillouzo A, Tuschl G, Li AP, LeCluyse E, Groothuis GMM, and Hengstler JG (2007) Primary hepatocytes: current understanding of the regulation of metabolic enzymes and transporter proteins, and pharmaceutical practice for the use of hepatocytes in metabolism, enzyme induction, transporter, clearance, and hepatotoxicity studies. *Drug Metab Rev* 39:159–234.

Kmieć Z (2001) Cooperation of liver cells in health and disease. *Adv Anat Embryol Cell Biol* 161:III–XIII, 1–151.

Krähenbühl L, Lang C, Lüdes S, Seiler C, Schäfer M, Zimmermann A, and Krähenbühl S (2003) Reduced hepatic glycogen stores in patients with liver cirrhosis. *Liver Int* 23:101–109.

Liew CY, Lim YC, and Yap CW (2011) Mixed learning algorithms and features ensemble in hepatotoxicity prediction. *J Comput Aided Mol Des* 25:855–871.

Lütgehetmann M, Mancke LV, Volz T, Helbig M, Allweiss L, Bornscheuer T, Pollok JM, Lohse AW, Petersen J, Urban S, and Dandri M (2012) Humanized chimeric uPA mouse model for the study of hepatitis B and D virus interactions and preclinical drug evaluation. *Hepatology* 55:685–694.

Melgert BN, Olinga P, Weert B, Slooff MJ, Meijer DK, Poelstra K, and Groothuis GM (2001) Cellular distribution and handling of liver-targeting preparations in

human livers studied by a liver lobe perfusion. *Drug Metab Dispos* 29:361–367.

Monbaliu D and Brassil J (2010) Machine perfusion of the liver: past, present and future. *Curr Opin Organ Transplant* 15:160–166.

Mueller D, Tascher G, Müller-Vieira U, Knobeloch D, Nuessler AK, Zeilinger K, Heinzle E, and Noor F (2011) In-depth physiological characterization of primary human hepatocytes in a 3D hollow-fiber bioreactor. *J Tissue Eng Regen Med* 5:e207–218.

Nelson PK, Mathers BM, Cowie B, Hagan H, Des Jarlais D, Horyniak D, and Degenhardt L (2011) Global epidemiology of hepatitis B and hepatitis C in people who inject drugs: results of systematic reviews. *Lancet* 378:571–583.

Pennington CR, Ross PE, and Bouchier IA (1977) Serum bile acids in the diagnosis of hepatobiliary disease. *Gut* 18:903–908.

Rahbari NN, Mehrabi A, Mollberg NM, Müller SA, Koch M, Büchler MW, and Weitz J (2011) Hepatocellular carcinoma: current management and perspectives for the future. *Ann Surg* 253:453–469.

Tateno C, Yoshizane Y, Saito N, Kataoka M, Utoh R, Yamasaki C, Tachibana A, Soeno Y, Asahina K, Hino H, Asahara T, Yokoi T, Furukawa T, and Yoshizato K (2004) Near completely humanized liver in mice shows human-type metabolic responses to drugs. *Am J Pathol* 165:901–912.

Taylor MJ and Baicu SC (2010) Current state of hypothermic machine perfusion preservation of organs: The clinical perspective. *Cryobiology* 60:S20–35.

Thewes S, Reed H-K, Grosse-Siestrup C, Groneberg DA, Meissler M, Schaller M, and Hube B (2007) Haemoperfused liver as an ex vivo model for organ invasion of Candida albicans. *J Med Microbiol* 56:266–270.

Vanwolleghem T, Libbrecht L, Hansen BE, Desombere I, Roskams T, Meuleman P, and Leroux-Roels G (2010) Factors determining successful engraftment of hepatocytes and susceptibility to hepatitis B and C virus infection in uPA-SCID mice. *J Hepatol* 53:468–476.

Vogel T, Brockmann JG, and Friend PJ (2010) Ex-vivo normothermic liver perfusion: an update. *Curr Opin Organ Transplant* 15:167–172.

Watkins PB (2011) Drug safety sciences and the bottleneck in drug development. *Clin Pharmacol Ther* 89:788–790.

Zeilinger K, Schreiter T, Darnell M, Söderdahl T, Lübberstedt M, Dillner B, Knobeloch D, Nüssler AK, Gerlach JC, and Andersson TB (2011) Scaling down of a clinical three-dimensional perfusion multicompartment hollow fiber liver bioreactor developed for extracorporeal liver support to an analytical scale device useful for hepatic pharmacological in vitro studies. *Tissue Eng Part C Methods* 17:549–556.

FOOTNOTE PAGE

Financial Support

This work was supported by the DFG [CA267/6-1; CA267/8-1], the Wilhelm-Laupitz-Foundation (A.C.), and by ZIM grants [KF2531501AJ9 (T.S., G.M., G.G., A.C.) and KF2531701AJ9 (R.K.G., M.F.)] by the Federal Ministry of Economics and Technology (BMWi), Germany, *via* the Consortium of Industrial Research Associations (AiF).

Competing Financial Interests

T.S., G.M., R.K.G., M.F. and A.C. have submitted a patent application specifying this perfusion system to the European Patent Office.

Citation of meeting abstract:

Schreiter T, Marquitan G, Darnell M, Sowa J-P, Bröcker-Preuss M, Andersson TB, Baba HA, Furch M, Rauen U, Mathé Z, Treckmann J, Gieseler RK, Gerken G, Canbay A. Characteristics of human non-cirrhotic and cirrhotic liver sections in a novel ex vivo perfusion system. 28th Annual Convention of the German Association for the Study of the Liver (GASL). January 27 to 28, 2012. Hamburg, Germany. Presentation on 2012-01-27. Z Gastroenterol 2012; 50: P2_28.

Reprint requests should be addressed to the corresponding author:

Ali Canbay, M.D.

Clinic for Gastroenterology and Hepatology

University Hospital Essen

Hufelandstr. 55

45122 Essen, Germany

E-mail: ali.canbay@uni-due.de

FIGURE LEGENDS

Figure 1 | Schematic diagram of the perfusion assembly.

Figure 2 | H&E stains of NC tissue (A-C) and CL tissue (D-F) upon retrieval (A, D) and after 6-h perfusion of a perfused area (B, E) *vs*. a non-perfused area (C, F). The scale bar corresponds to 1 mm.

Figure 3 | General hepatic metabolic parameters. Glucose (A), lactate (B) and oxygen (C) consumption in non-cirrhotic (n=10) and cirrhotic (n=12) liver specimens were determined in the perfusates. Values were normalized per gram of tissue and are displayed as means ± SEM. Missing data sets are due to mandatory maintenance of the device.

Figure 4 | Hepatic synthesis parameters. Production of urea (A), bile acids (B) and albumin (C) by non-cirrhotic (n=10) and cirrhotic liver (n=12) specimens were measured. Data were normalized per gram of tissue and are shown as means ± SEM. Grubb analysis identified the missing data set of bile acids as an outlier (cf. Supplementary Figure 2).

Figure 5 | Liver enzymes released during perfusion. Release of the cell integrity markers LDH (A), GLDH (B), AST (C), ALT (D) and γGT (E) by non-cirrhotic (n=10) and cirrhotic liver (n=12) specimens. Data were normalized per gram of tissue and are shown as means ± SEM.

Figure 6 | Cell death parameters throughout tissue perfusion. Display of (A) marker M65, indicating cell death by both necrosis and apoptosis; (B) marker M30, selectively indicating apoptosis, and (C) ratio of the M30/M65 levels (c). Values were normalized per gram of tissue and are displayed as means ± SEM.

Figure 7 | Concentrations of cytochrome P450 (CYP) metabolites (phase-I products) in liver tissue perfusate. The activities of CYP1A1/1A2 (A), CYP3A4 (B) and CYP2C9 (C) were assessed by adding the respective model substrates to the perfusion medium. In order to better illustrate the short time periods during which phase-I reactions occurred (early time periods), the respective curve sections are displayed separately (D-F). Hence, late time periods correlate with occurrence of phase-II reactions. The corresponding areas under the curves are given in panels (G-J). Lower AUC values in the phase-I diagrams indicate higher phase-II reactivities.

Figure 8 | Immunohistochemical stains of CYP1A1, CYP3A4 or CYP2C9 in NC and CL tissue. Depicted are representative photomicrographs of NC and CL tissue for each of the three isoenzymes before and after the perfusion experiment. Positive areas were more restricted in CL than in NC samples. After 6 h of perfusion the positive stained regions were reduced in both NC and CL compared to the pre-perfusion status. The scale bar corresponds to 100 µm.

JPET Fast Forward. Published on June 6, 2012 as DOI: 10.1124/jpet.112.194167
This article has not been copyedited and formatted. The final version may differ from this version.

TABLES

Table 1 | General characteristics of patients and derived liver samples.

Number	Surgical intervention	Underlying disease	Gender / Age	Sample weight [g]	Experimental intervention*
NC-1	Right-side hemihepatectomy	Klatskin tumor	f / 61	55	15 mM $NaHCO_3$
NC-2	Left-side hemihepatectomy	Hemangioma	f / 38	18	3 mM NaH_2PO_4
NC-3	Right-side hemihepatectomy	Klatskin tumor	f / 60	70	15 mM $NaHCO_3$
NC-4	Left-side partial resection	Metastasized colon carcinoma	f / 75	19	2 mM NaH_2PO_4 12.5 mM $NaHCO_3$
NC-5	Right-side hemihepatectomy	Metastasized colon carcinoma	m / 43	45	17.5 mM $NaHCO_3$
NC-6	Right-side hemihepatectomy	Metastasized rectal carcinoma	m / 52	55	35 mM $NaHCO_3$
NC-7	Right-side hemihepatectomy	Metastasized soft palate carcinoma	m / 55	54	20 mM $NaHCO_3$
NC-8	Explantation	Hepatocellular carcinoma	f / 59	56	30 mM $NaHCO_3$
NC-9	Right-side hemihepatectomy	Cholangiocellular carcinoma	m / 70	55	22.5 mM $NaHCO_3$
NC-10	Explantation	Hepatocellular carcinoma	m / 59	50	25 mM $NaHCO_3$
CL-1	Explantation	Hepatitis C	f / 61	40	30 mM $NaHCO_3$
CL-2	Explantation	Hepatitis C	m / 50	25	15 mM $NaHCO_3$
CL-3	Explantation	Hepatitis C	m / 51	48	30 mM $HaHCO_3$ 150 mg/dL Glucose
CL-4	Explantation	Ethanol toxicity	m / 48	42	30 mM $NaHCO_3$
CL-5	Explantation	Hepatitis C	m / 61	55	55 mM $NaHCO_3$
CL-6	Explantation	Hepatitis C	m / 66	55	40 mM $NaHCO_3$
CL-7	Explantation	Primary biliary cirrhosis	f / 51	32	35 mM $NaHCO_3$
CL-8	Explantation	Hepatitis C	m / 61	38	70 mM $NaHCO_3$ 2x 200 mg/dL Glucose
CL-9	Explantation	Hepatitis C	m / 41	31	10 mM $NaHCO_3$
CL-10	Explantation	Hepatitis C	m / 57	57	42.5 mM $NaHCO_3$
CL-11	Explantation	Ethanol toxicity	m / 58	57	52.5 mM $NaHCO_3$
CL-12	Explantation	Ethanol toxicity	f / 34	55	50 mM $NaHCO_3$ 200 mg/dL Glucose

NC: non-cirrhotic, CL: cirrhotic liver tissue. *: Experimental intervention indicates the replenishment of glucose when the perfusate value went below 40 mg/dL and how much buffer was totally necessary during 6 h to maintain the pH around 7.35 in 200ml volume of perfusate.

JPET Fast Forward. Published on June 6, 2012 as DOI: 10.1124/jpet.112.194167
This article has not been copyedited and formatted. The final version may differ from this version.

Table 2 | Calculation of areas under the curves (AUCs, A) and slope values (B) from non-cirrhotic (NC) and cirrhotic (CL) liver samples. AUCs indicate overall production or consumption during the experimentation period. AUC ratios demonstrate the factor by which the values differed between NC and CL samples. A slope was indicated when at least one r value of the Pearsson correlation analysis was >0.9 (not shown) although the correlation in the related graph did not appear linear. The difference of the slopes is given as the *P* value.

A

Parameter	Area under curve (AUC)		AUC ratio
	NC	CL	NC / CL
Glucose [mg x h x dL^{-1} x g^{-1}]	8.03	1.76	4.56
Lactate [mmol x h x L^{-1} x g^{-1}]	1.31	2.45	0.53
Oxygen [µL x h x min^{-1} x g^{-1}]	7.55	6.59	1.14
Urea [mg x h x dL^{-1} x g^{-1}]	0.55	0.52	1.05
Albumin [µg x h x mL^{-1} x g^{-1}]	14	14.69	0.95
Bile acids [µmol x h x L^{-1} x g^{-1}]	0.41	0.85	0.49
LDH [U x h x L^{-1} x g^{-1}]	374.3	224.5	1.67
GLDH [U x h x L^{-1} x g^{-1}]	31.37	8.35	3.76
AST [U x h x L^{-1} x g^{-1}]	276.5	222.9	1.24
ALT [U x h x L^{-1} x g^{-1}]	191	67.54	2.83
gGT [U x h x L^{-1} x g^{-1}]	2.78	1.17	2.37
M65 [U x h x L^{-1} x g^{-1}]	6278	11869	0.53
M30 [U x h x L^{-1} x g^{-1}]	146.3	316.2	0.46

JPET Fast Forward. Published on June 6, 2012 as DOI: 10.1124/jpet.112.194167
This article has not been copyedited and formatted. The final version may differ from this version.

B

Parameter	Slope (average production/h)		Difference of slopes
	NC	CL	*P*
Glucose [mg x dL^{-1} x g^{-1} x h^{-1}]	r < 0.9	r < 0.9	
Lactate [mmol x L^{-1} x g^{-1} x h^{-1}]	0.056 ± 0.005	0.122 ± 0.008	< 0.0001
Oxygen [µL x min^{-1} x g^{-1} x h^{-1}]	r < 0.9	r < 0.9	
Urea [mg x dL^{-1} x g^{-1} x h^{-1}]	0.022 ± 0.003	0.016 ± 0.001	0.0609
Albumin [µg x mL^{-1} x g^{-1} x h^{-1}]	0.367 ± 0.076	0.154 ± 0.126	0.1705
Bile acids [µmol x L^{-1} x g^{-1} x h^{-1}]	0.015 ± 0.003	0.017 ± 0.003	0.7225
LDH [U x L^{-1} x g^{-1} x h^{-1}]	22.79 ± 3.19	7.696 ± 1.41	< 0.0001
GLDH [U x L^{-1} x g^{-1} x h^{-1}]	2.98 ± 0.52	0.576 ± 0.12	< 0.0001
AST [U x L^{-1} x g^{-1} x h^{-1}]	17.28 ± 2.65	8.656 ± 1.52	0.0038
ALT [U x L^{-1} x g^{-1} x h^{-1}]	12.48 ± 2.16	2.002 ± 0.54	< 0.0001
gGT [U x L^{-1} x g^{-1} x h^{-1}]	0.097 ± 0.022	0.023 ± 0.005	0.0004
M65 [U x L^{-1} x g^{-1} x h^{-1}]	207.5 ± 66.6	399.4 ± 194.3	0.3876
M30 [U x L^{-1} x g^{-1} x h^{-1}]	4.83 ± 2.15	13.86 ± 3.99	0.0617

Figure 1

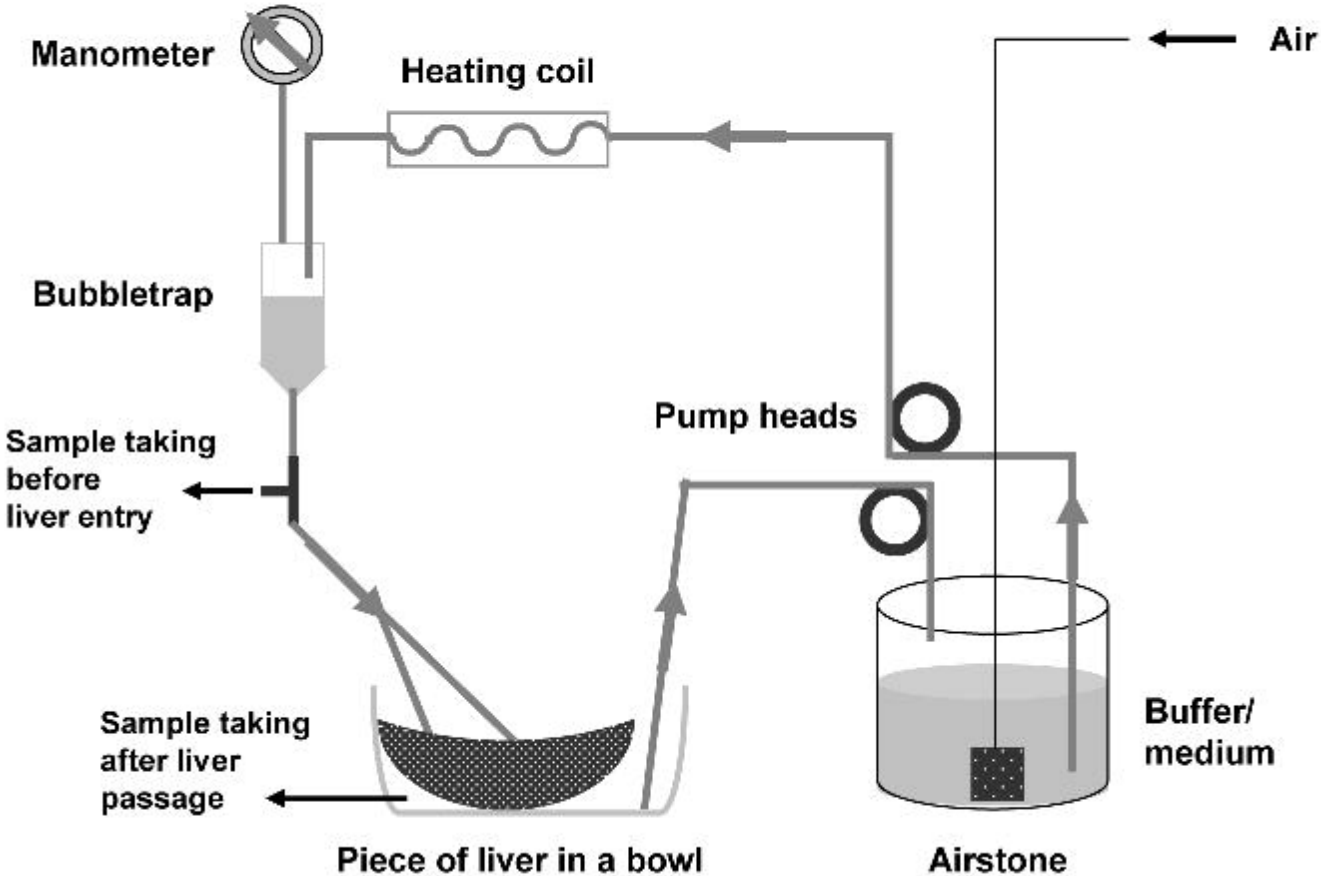
Manometer
Heating coil
Air
Bubbletrap
Pump heads
Sample taking
before
liver entry
Sample taking
after liver
passage
Buffer/
medium
Piece of liver in a bowl
Airstone

Figure 2

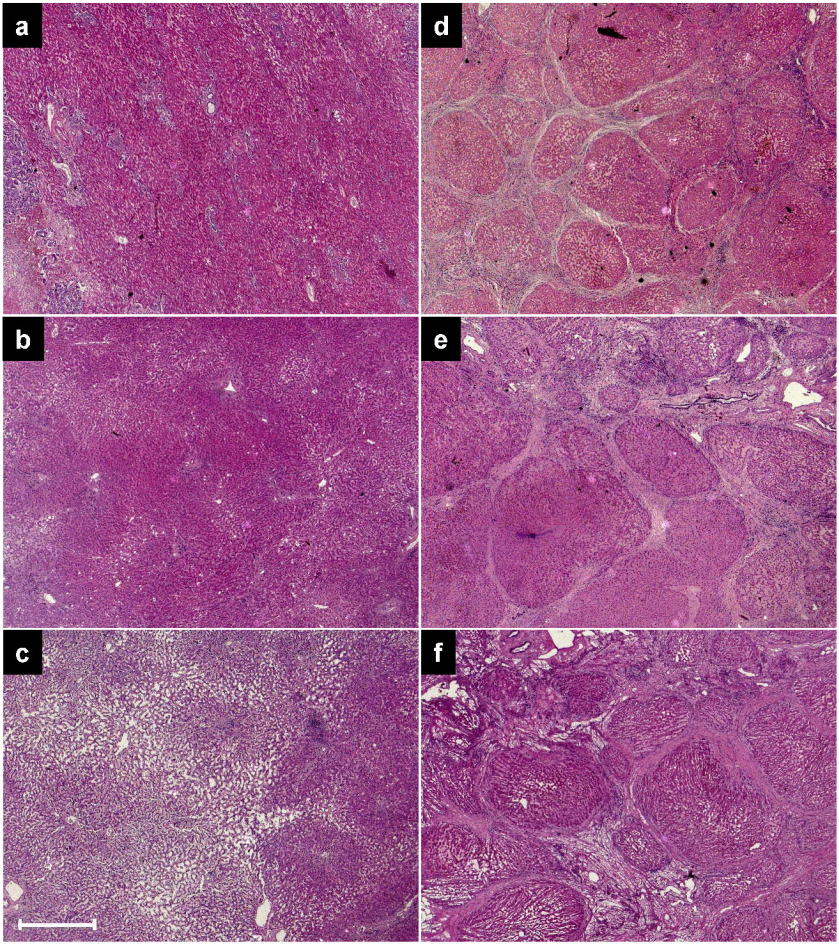

Figure 3

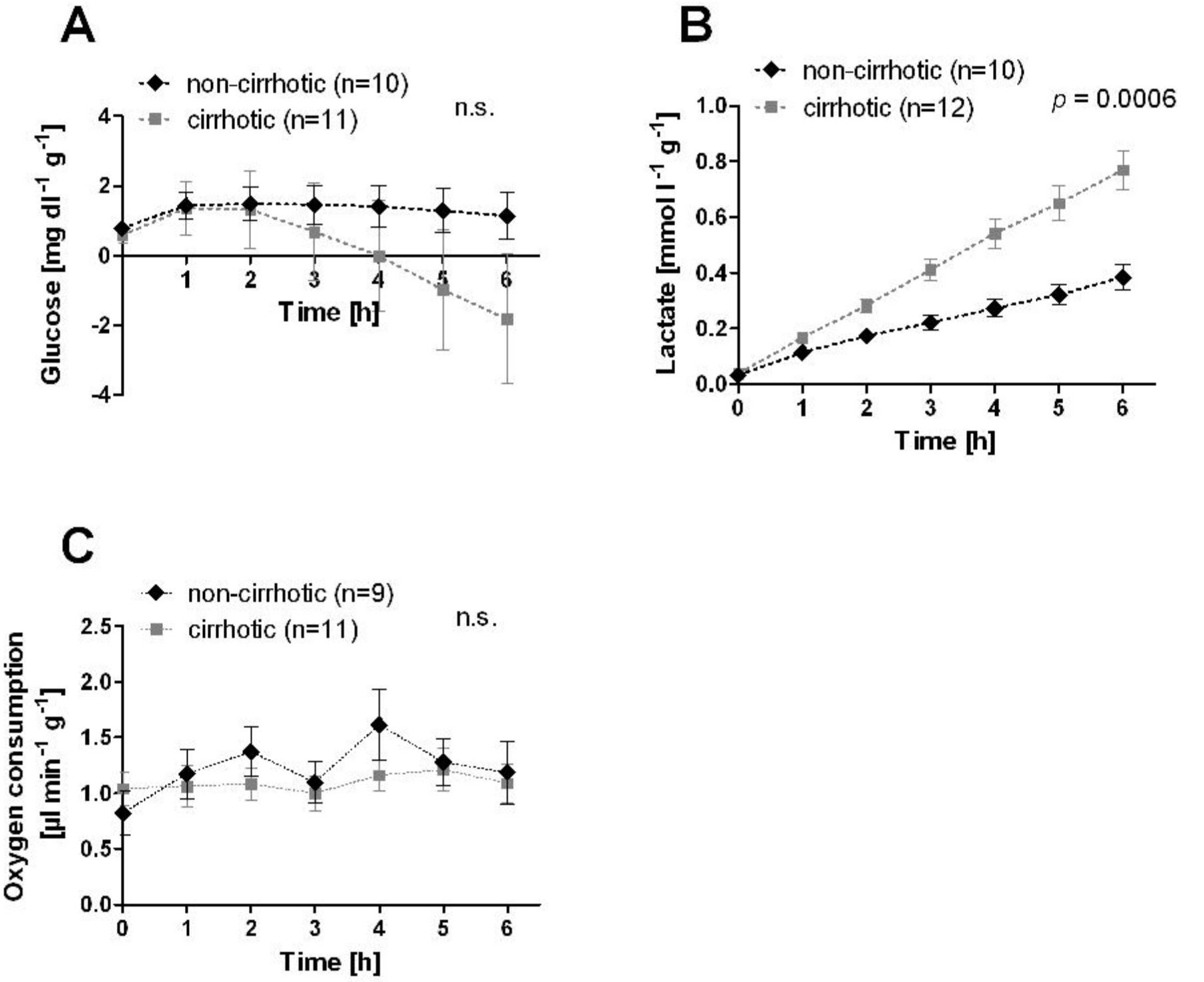
A
non-cirrhotic (n=10)
cirrhotic (n=11)
n.s.
Glucose [mg dl-1 g-1]
Time [h]
B
non-cirrhotic (n=10)
cirrhotic (n=12)
p = 0.0006
Lactate [mmol l-1 g-1]
Time [h]
C
non-cirrhotic (n=9)
cirrhotic (n=11)
n.s.
Oxygen consumption [µl min-1 g-1]
Time [h]

Figure 4

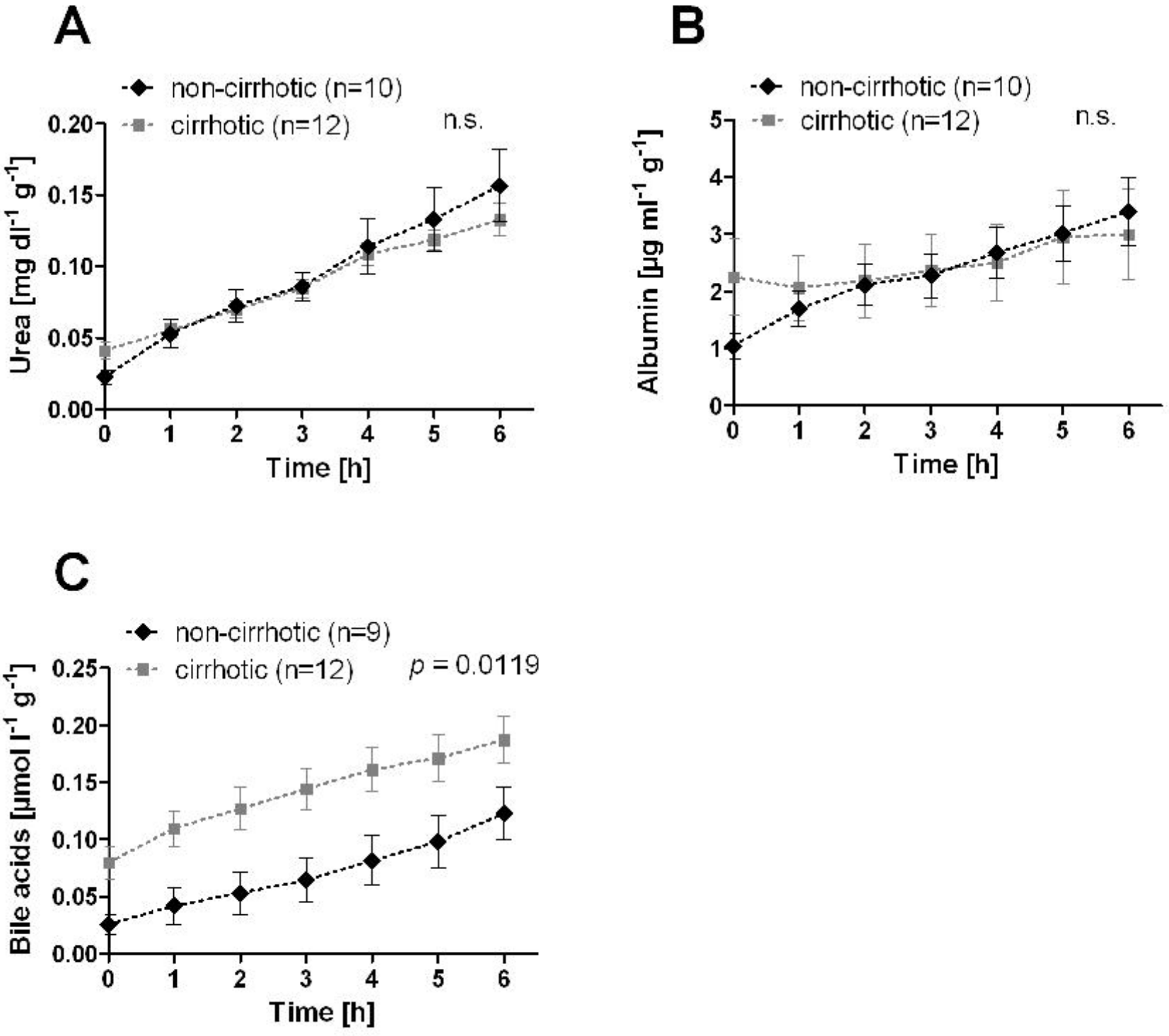
A
non-cirrhotic (n=10)
cirrhotic (n=12)
n.s.
Urea [mg dl-1 g-1]
0.20
0.15
0.10
0.05
0.00
0
1
2
3
4
5
6
Time [h]
B
non-cirrhotic (n=10)
cirrhotic (n=12)
n.s.
Albumin [µg ml-1 g-1]
5
4
3
2
1
0
Time [h]
C
non-cirrhotic (n=9)
cirrhotic (n=12)
p = 0.0119
Bile acids [µmol l-1 g-1]
0.25
0.20
0.15
0.10
0.05
0.00
Time [h]

Figure 5

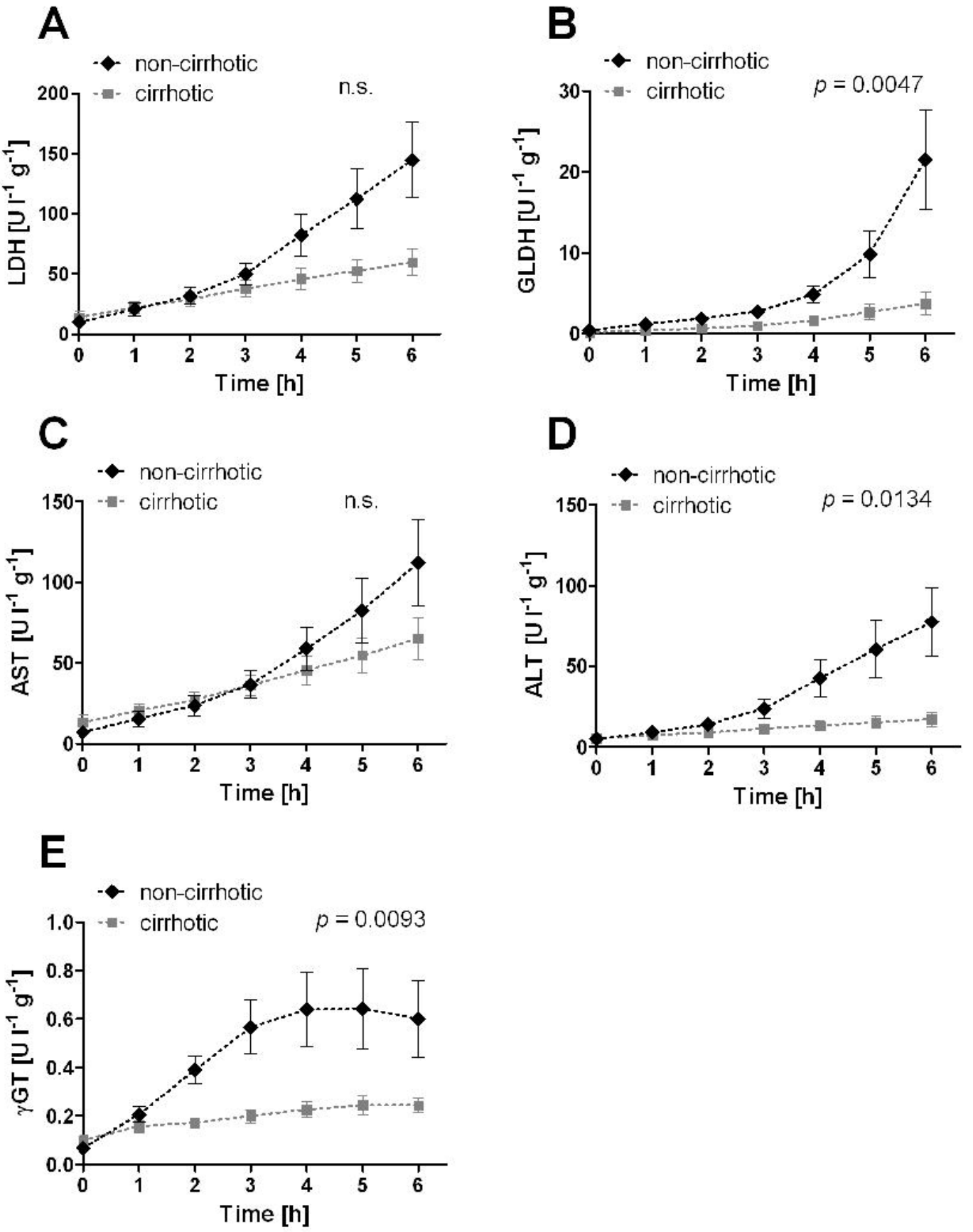
A
non-cirrhotic
cirrhotic
n.s.
LDH [U l-1 g-1]
Time [h]
B
non-cirrhotic
cirrhotic
p = 0.0047
GLDH [U l-1 g-1]
Time [h]
C
non-cirrhotic
cirrhotic
n.s.
AST [U l-1 g-1]
Time [h]
D
non-cirrhotic
cirrhotic
p = 0.0134
ALT [U l-1 g-1]
Time [h]
E
non-cirrhotic
cirrhotic
p = 0.0093
γGT [U l-1 g-1]
Time [h]

Figure 6

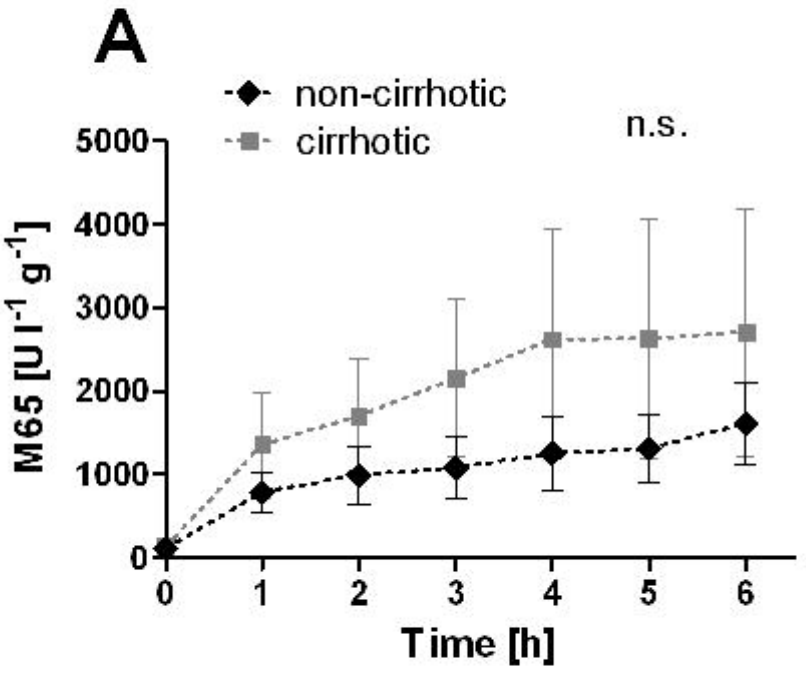
A
non-cirrhotic
cirrhotic
n.s.
M65 [U l-1 g-1]
5000
4000
3000
2000
1000
0
0
1
2
3
4
5
6
Time [h]

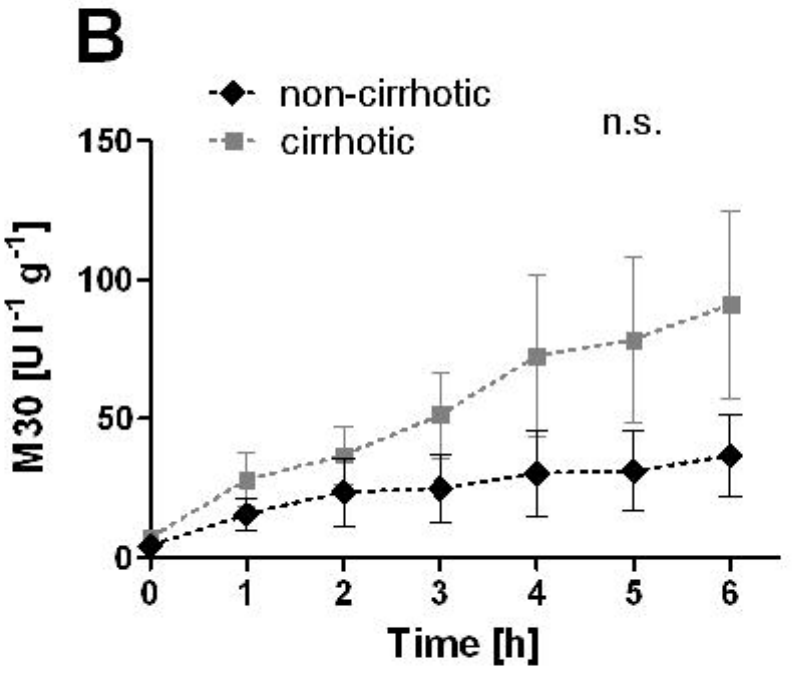
B
non-cirrhotic
cirrhotic
n.s.
M30 [U l-1 g-1]
150
100
50
0
0
1
2
3
4
5
6
Time [h]

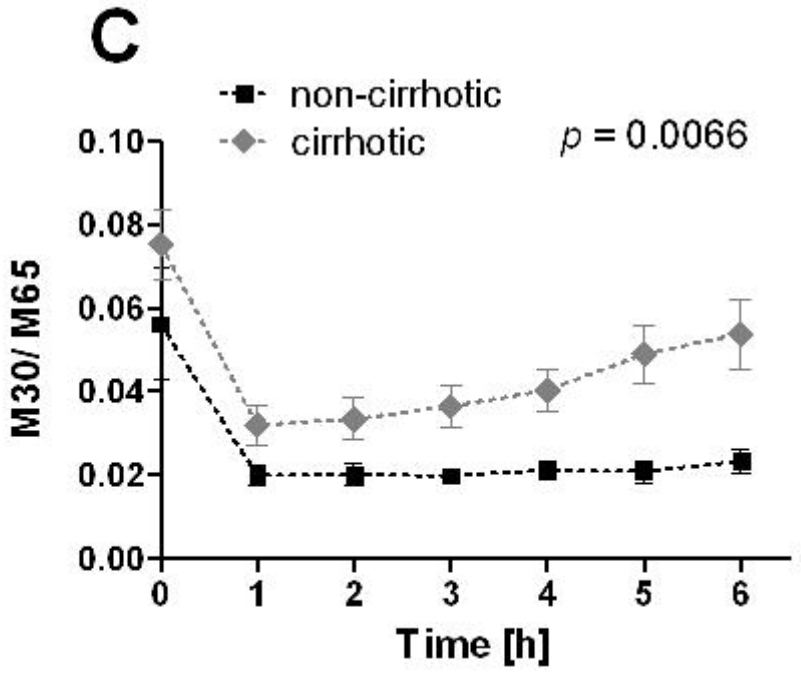
C
non-cirrhotic
cirrhotic
p = 0.0066
M30/ M65
0.10
0.08
0.06
0.04
0.02
0.00
0
1
2
3
4
5
6
Time [h]

Figure 7

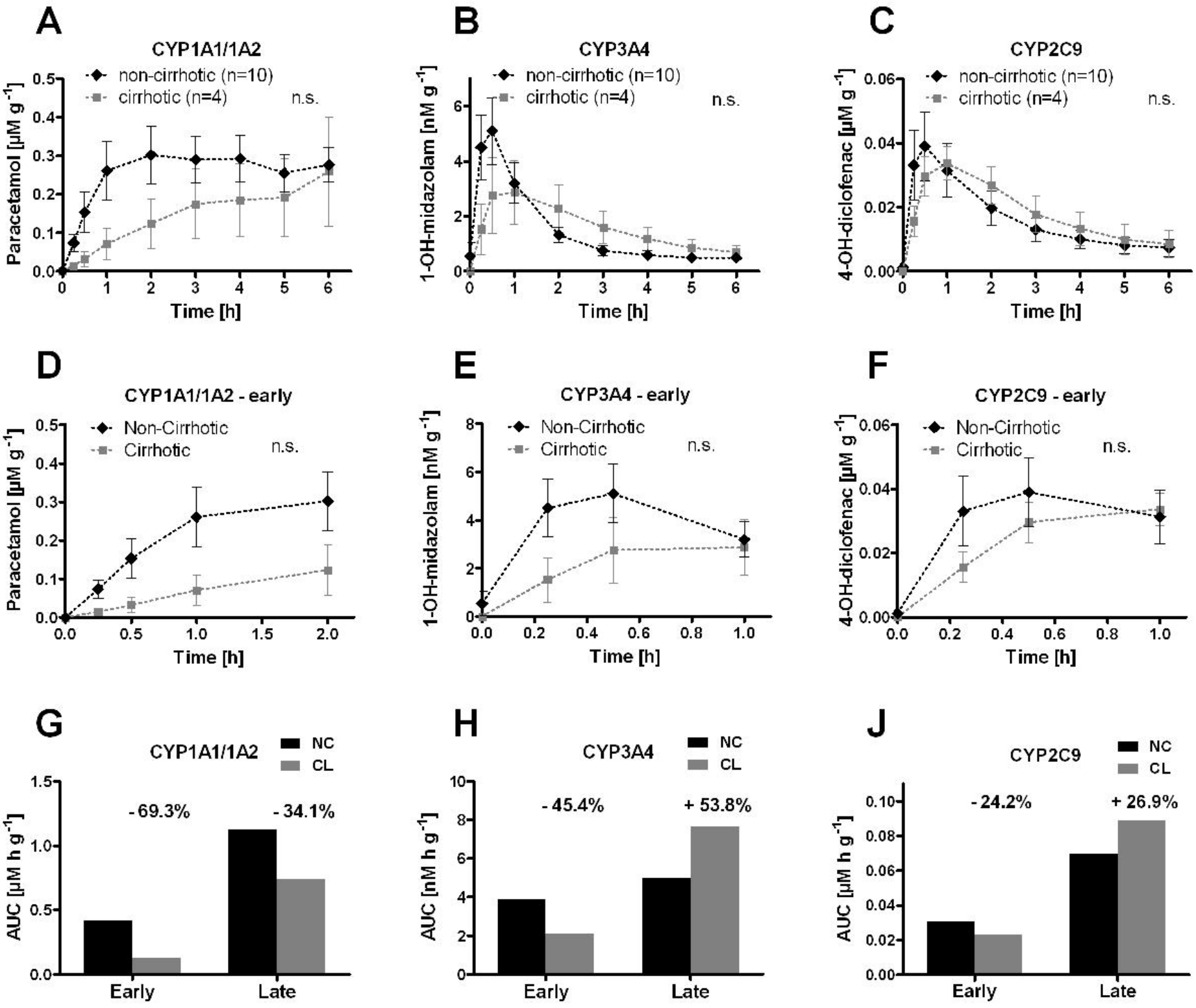
A
CYP1A1/1A2
non-cirrhotic (n=10)
cirrhotic (n=4)
n.s.
Paracetamol [µM g-1]
Time [h]
B
CYP3A4
non-cirrhotic (n=10)
cirrhotic (n=4)
n.s.
1-OH-midazolam [nM g-1]
Time [h]
C
CYP2C9
non-cirrhotic (n=10)
cirrhotic (n=4)
n.s.
4-OH-diclofenac [µM g-1]
Time [h]
D
CYP1A1/1A2 - early
Non-Cirrhotic
Cirrhotic
n.s.
Paracetamol [µM g-1]
Time [h]
E
CYP3A4 - early
Non-Cirrhotic
Cirrhotic
n.s.
1-OH-midazolam [nM g-1]
Time [h]
F
CYP2C9 - early
Non-Cirrhotic
Cirrhotic
n.s.
4-OH-diclofenac [µM g-1]
Time [h]
G
CYP1A1/1A2
NC
CL
-69.3%
-34.1%
AUC [µM h g-1]
Early
Late
H
CYP3A4
NC
CL
-45.4%
+53.8%
AUC [nM h g-1]
Early
Late
J
CYP2C9
NC
CL
-24.2%
+26.9%
AUC [µM h g-1]
Early
Late

Figure 8

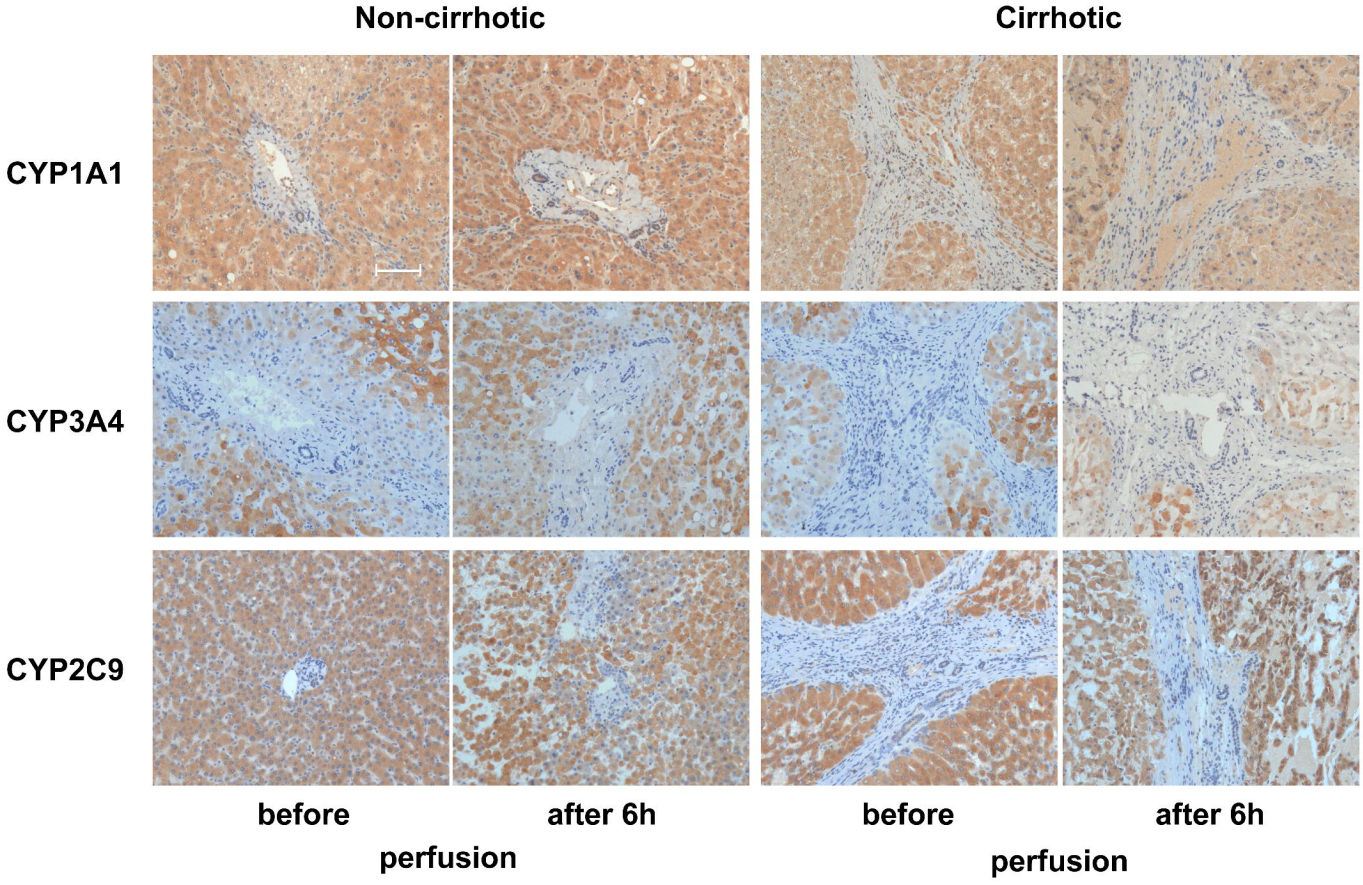
Non-cirrhotic
Cirrhotic
CYP1A1
CYP3A4
CYP2C9
before
after 6h
perfusion
before
after 6h
perfusion